ELSEVIER

On the mechanism of the P2–Na$_{0.70}$CoO$_2$→O2–LiCoO$_2$ exchange reaction—Part I: proposition of a model to describe the P2–O2 transition

F. Tournadre,[a] L. Croguennec,[a,*] I. Saadoune,[a,b] D. Carlier,[a] Y. Shao-Horn,[a] P. Willmann,[c] and C. Delmas[a]

[a] Institut de Chimie de la Matière Condensée de Bordeaux-CNRS and Ecole Nationale Supérieure de Chimie et Physique de Bordeaux, Université Bordeaux I, 87 Avenue du Dr A. Schweitzer, 33608 Pessac Cedex, France
[b] LCME, Département de Chimie, Faculté des Sciences et Techniques, Avenue Abdelkrim, B.P. 549, 40000 Marrakech, Morocco
[c] Centre National d'Etudes Spatiales, 18 Avenue Edouard Belin, 31401 Toulouse Cedex 4, France

Abstract

A model was proposed to describe the exchange reaction of sodium by lithium in P2 crystals. The exchange consists on the formation of nucleation centers and then on the growth of O2 domains in P2 crystals from these nucleation centers. Octahedral environments for lithium ions are obtained when one slab over two glides by (2/3,1/3,0) or by (1/3,2/3,0) in P2 structure. The existence of two different gliding vectors should lead to stacking faulted structures that can be simulated using DIFFaX software. The comparison of simulated and experimental XRD patterns for O2–LiCoO$_2$ (ex-Na$_{0.7}$CoO$_2$) has shown that in that case the growth of the O2 domains in the P2 crystals is faster than the formation of nucleation centers.
© 2004 Elsevier Inc. All rights reserved.

1. Introduction

Lamellar LiCoO$_2$ can exhibit two different stackings, depending on the synthesis method. The well known O3–LiCoO$_2$ phase, used as positive electrode material in most of the commercialized lithium-ion batteries, is obtained by high temperature solid-state reaction, whereas the metastable O2–LiCoO$_2$ phase was first prepared 20 years ago in our lab from P2–Na$_{0.70}$CoO$_2$, using ion exchange reaction [1]. At that time, Mendiboure et al. studied lithium deintercalation from the O2–LiCoO$_2$ phase by X-ray diffraction (XRD) [2]. All the phases are named in this paper according to the packing designation commonly used for the layered oxides: the letters P, T and O describe the alkali ion environment (prismatic, tetragonal or octahedral, re-

spectively) and the numbers 1, 2, 3… give the number of slabs required to describe the hexagonal cell [3].

Recently, Paulsen et al. were also interested in O2-type structures. In a first step, they studied O2–LiMnO$_2$ and showed that contrary to O3–LiMnO$_2$, the O2–LiMnO$_2$ phase does not convert into a spinel structure during cycling [4]. But, due to poor electrochemical performances, this phase was shown not to be promising as positive electrode material for Li-ion batteries. In a second step, they extended their work to the O2–LiCoO$_2$ system [5]. Then, they focused their interest on Li$_{2/3}$Ni$_{1/3}$Mn$_{2/3}$O$_2$, prepared by ion exchange from P2−Na$_{2/3}$Ni$_{1/3}$Mn$_{2/3}$O$_2$ [6,7], and on cobalt substituted phases such as the Li$_{2/3}$[Ni$_{1/3-x}$Co$_x$Mn$_{2/3}$]O$_2$ phases ($0 < x \leqslant 1/3$) [8] and the Li$_{2/3}$[Ni$_{1/3-x/2}$Co$_x$Mn$_{2/3-x/2}$]O$_2$ phases ($0 < x \leqslant 2/3$), where, in these latters, all manganese ions are tetravalent [9]. In this system, a T$^{\#}$2 phase was obtained for both end members while intermediate compositions exhibit stacking faulted structures and/or incomplete ion exchange

*Corresponding author. Fax: +33-540006698.
E-mail address: crog@icmcb.u-bordeaux1.fr (L. Croguennec).

[8,10]. Lu et al. showed that in the $Li_{2/3}[Ni_{1/3-x}Co_xMn_{2/3}]O_2$ system stacking faulted structures can be explained by T2–O2 intergrowths for small amounts of cobalt substitution ($x = 1/24$) and by O6 or O2 stacking faulted structures for larger cobalt amounts ($x > 1/12$) [10]. In a first attempt to explain the difference in efficiency for the ionic exchange, Paulsen et al. suggested that the existence of a Ni/Mn ordering in the slab for $Li_{2/3}Ni_{1/3}Mn_{2/3}O_2$ (shown by neutron diffraction [11]) could imply an easy ionic exchange and could thus lead to a high-crystallized $T^{\#}2$ structure. However, no long range superlattice ordering was evidenced for the $T^{\#}2$–$Li_{2/3}[Co_{2/3}Mn_{1/3}]O_2$ phase [9].

With the aim to better understand the mechanism of the ionic exchange, we studied this reaction in a simple case. $P2$–$Na_{0.70}CoO_2$ transforms to $LiCoO_2$ after ion exchange of Na^+ by Li^+ in an LiCl/LiOH (1:1) aqueous

solution [12]. As the cobalt ions are not stable at the $4+$ oxidation state, the reaction induces also the reduction of the material which leads to the $LiCoO_2$ formulae. This $P2 \rightarrow O2$ transition results from a slab gliding, as shown in Fig. 1 one slab over two glides by (1/3,2/3,0). In order to describe easily these layered structures and polyhedra stacking, sections along the (110) plane will be used (Fig. 1a). Fig. 1b gives a comparison of the perspective view and of the section along the (110) plane. In this section, the octahedra are represented by parallelograms, the tetrahedra by triangles and the pyramidal prisms by rectangles. As also highlighted in Fig. 1b, in this section a face shared by two octahedra appears as a line while an edge appears as a point. The driving force for this $P2 \rightarrow O2$ transition is the formation of octahedral environments for the lithium ions, that are too small to be stabilized in trigonal prismatic
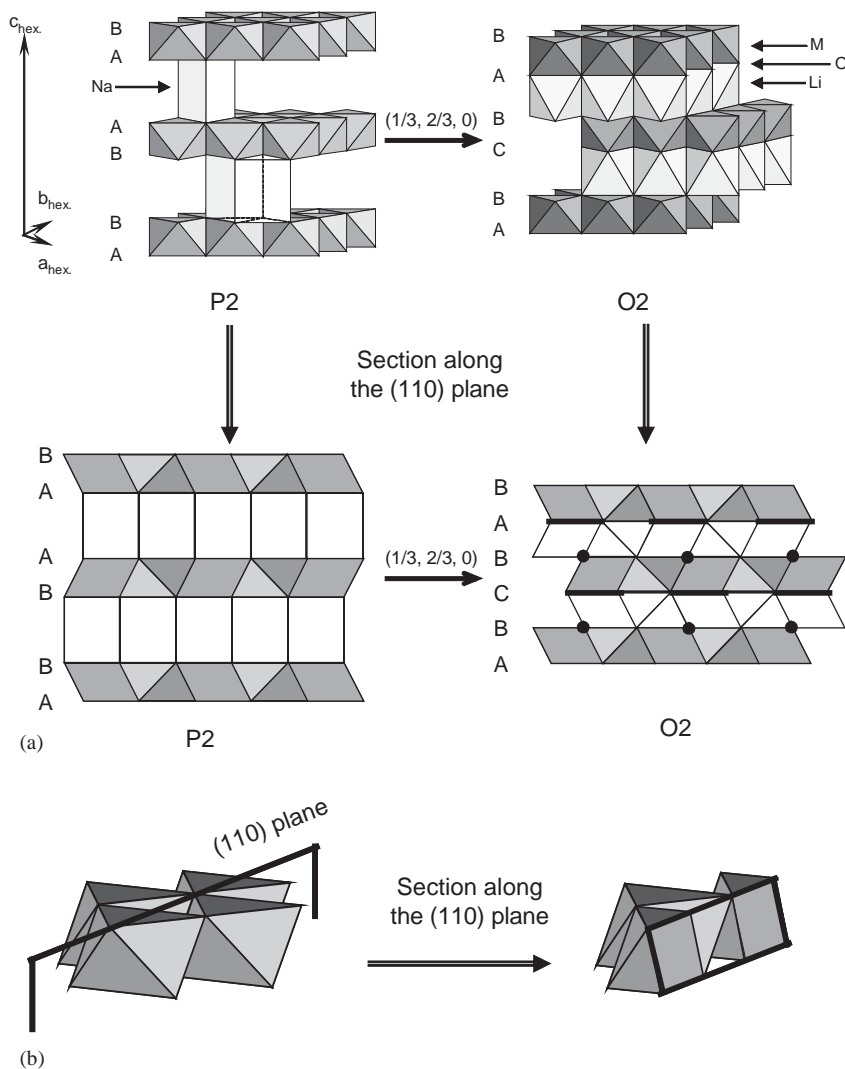

Fig. 1. (a) Slab gliding involved in the $P2 \rightarrow O2$ structural transformation, represented in 3D perspective and in 2D along the (110) direction. A common face appears as a line shared between two parallelograms while a common edge appears as a point in the section. (b) Section along the (110) plane of MO_2 slab.

sites: these LiO_6 octahedra share one face on one side and three edges on the other side with MO_6 octahedra (*M*: transition metal ion). Note that exactly the same O2 structure is obtained when one slab over two glides by (2/3,1/3,0). In this paper, we will propose a general model that allows to consider for the P2–O2 transition how occur the exchange reactions at the microscopic scale in a given crystallite. The nucleation of the O2 phase within a P2 crystallite can occur in several parts of the crystal with the two gliding vectors (1/3,2/3,0) and (2/3,1/3,0); therefore, extended defects can be formed at the boundaries between the various domains. The Part I of this paper is thus focused on the XRD patterns simulation in order to evidence the presence of defects and the relative importance of the nucleation and growing processes during a P2–O2 transition. The results of these simulations will be used to analyze the formation of $O2–LiCoO_2$ by considering its experimental XRD pattern. The Part II companion paper will present an in situ XRD study of the Na^+ by Li^+ exchange process in $P2–Na_{0.7}CoO_2$, which emphasizes the results of this first part.

2. Experimental

2.1. Phase preparation

The Na_xCoO_2 phases exhibit the P2 stacking for $0.64 < x < 0.74$ [13]. We chose the composition $x = 0.70$ to prepare this precursor phase. The $P2–Na_{0.70}CoO_2$ material was prepared by solid-state reaction from a mixture of Na_2O (Aldrich 99% min, 5% excess) and Co_3O_4 (obtained from $Co(NO_3)_2 \cdot 6H_2O$ Carlo Erba 99% min at 450°C for 12h under O_2). The mixture was ground and pelletized in an argon-filled dry box and then treated at 800°C under O_2 for 48h. The resulting material was finally quenched in air. The XRD study shows that a pure $P2–Na_{0.70}CoO_2$ phase was obtained. Its unit cell parameters ($a_{hex} = 2.833$ Å and $c_{hex} = 10.81$ Å) were in good agreement with the previously reported ones [12].

The ex situ exchange reaction was performed using the procedure reported by Paulsen et al. [6] with an LiCl/LiOH (1:1) solution in water (5 M). An excess of lithium was used (Li/Na = 10) and the exchange was carried out under refluxing conditions during 24h with an intermediate washing, drying and grinding. In that conditions $O2–LiCoO_2$ was obtained ($a_{hex} = 2.804$ Å, $c_{hex} = 9.540$ Å). As usually observed traces of the precursor Na_xCoO_2 phase remains in the sample.

2.2. X-ray diffraction

The XRD pattern of $O2–LiCoO_2$ was collected at room temperature from 5° to 120° (2θ) with an 0.02° step and a 40s counting time by step, using a Siemens

D5000 powder diffractometer with $CuK\alpha$ radiation and a graphite diffracted beam monochromator.

The simulation of XRD patterns was done using the DIFFaX program [14], which calculates the diffracted intensity versus the 2θ value for a given stacking of MO_2 slabs. In this study, two types of MO_2 slabs were used: *AB* and *BA* with for both $a_{hex} = 2.804$ Å, $c_{hex} = 9.540$ Å. These slabs were then packed along the *c*-axis with a given stacking vector, which possibly introduces stacking faults. All the simulations considered a random distribution of stacking faults. Note that as lithium, on the contrary to sodium, is a poor XRD scatterer, it was not considered for the simulations. Furthermore, the scattering factor taken for *M* was that of Co.

3. Results

3.1. Nucleation versus growing of the O2 domains in the P2 crystal

The nucleation that is at the origin of the P2→O2 transition can be associated, as shown in Fig. 2, either with the gliding of a single slab or with the gliding of a large block of the crystal. As a result, in the first case two interslab spaces are modified, whereas in the second case, only one interslab space is modified. Since the translation of a large block of the crystal appears not to be likely (reaction requiring too much energy), we have chosen to consider only the hypothesis that associates a nucleation center with the gliding of a single slab. However, in this case a single gliding leads to the formation of two octahedrally surrounded lithium interslab spaces instead of one in the other case, that induces a higher material stabilization for one slab gliding.

Then, it is useful to explain how the growing occurs. As shown in Fig. 3, when one slab of the P2 crystal has moved in a given direction (1/3,2/3,0) for example (arrow of Fig. 3a), the growing of the O2 domain requires that the following similar slabs moves in the same direction (as indicated by the arrows) to avoid the formation of LiO_6 octahedra sharing only faces with their neighboring MO_6 octahedra. The growing from one nucleation center leads thus to the formation of an O2 domain without defects.

Note that if there are several nucleation centers well separated within the same crystal, each of them can occur on the two types of slabs (*AB* or *BA*) with two gliding translations (1/3,2/3,0) or (2/3,1/3,0). The growing from each nucleation center leads to the formation of several O2 domains and, therefore, defects occur at the junction between two O2 domains. The structure of the final material strongly depends on the ratio between the growing and the nucleation speeds. If the growing of the O2 domains is fast, only a few nucleation
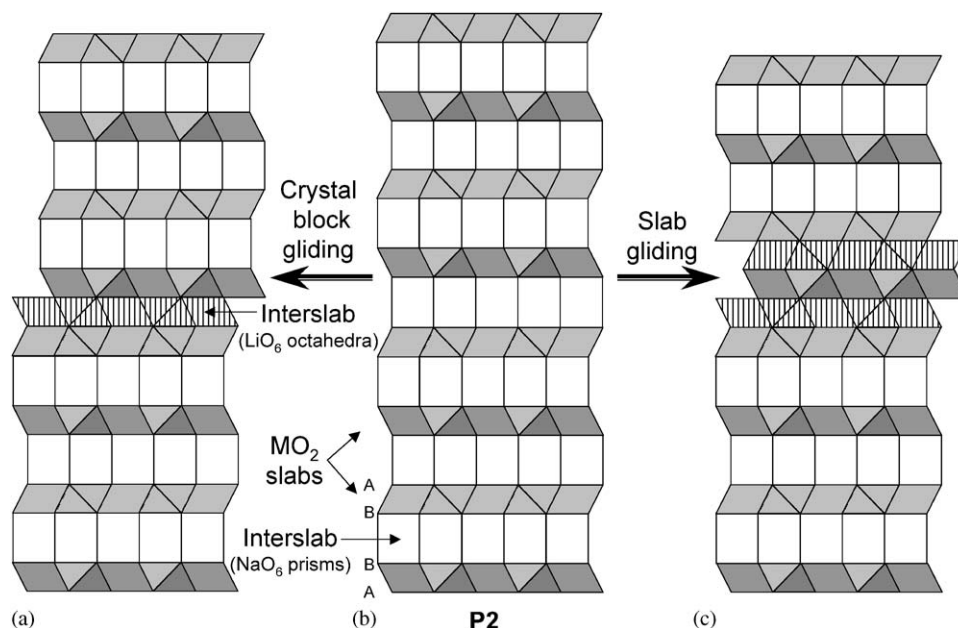
Fig. 2. Schematic representation projected along the (110) direction of the two hypotheses that can explain how the nucleation occurs. Two colors are used to distinguish the two types of slabs: the lighter slabs are *BA*-type slabs, whereas the darker slabs are *AB*-type slabs. Hatched polyhedra represent lithium containing interslab spaces.
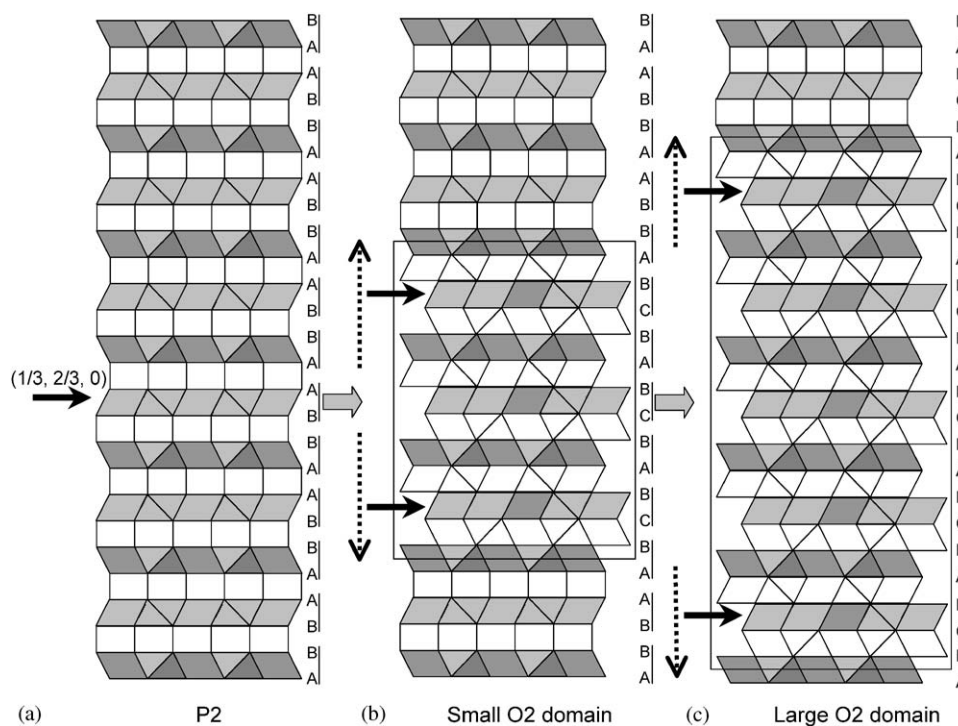
Fig. 3. An example of growing of an O2 domain in a P2 crystal, from a *BA*-type nucleation center in the (1/3,2/3,0) direction (black arrow). The same gliding vector is kept for the entire domain growth.

centers are created: the final crystal is thus made of large O2 domains with only a small amount of defects. On the contrary, if the growing of the O2 domains is slow, the nucleation centers have time to multiply: the final crystal is thus made of small O2 domains with a large amount of defects.

3.2. XRD patterns simulation

3.2.1. In the restricted hypothesis that only one type of slabs is nucleation center

In a first step, in order to simplify the structural model, we have considered that only one type of slabs

Fig. 4. An example of P2→O2 transition section along (110) plane. The lighter slabs are BA-type slabs, whereas the darker slabs are AB-type slabs. The nucleation centers are associated to only one type of slabs (BA for example), the gliding vectors (black arrows) being $(1/3, 2/3, 0)$ or $(2/3, 1/3, 0)$. The defects appear at the junction between two O2 domains. The classical O2 stacking is highlighted with polyhedra in bold lines and the stacking with defects with hatched polyhedra. Note that, for convenience, the sodium prisms have been drawn with the same height as the lithium octahedra.

Fig. 5. Scheme of the O2 structures using DIFFaX software for pure O2 phase (a) and for O2 stacking faulted phase (b). The vectors and their probabilities are also given.

Table 1
Structural description of the *AB*-type slabs (slab no. 1, slab no. 3,…,slab no. 11) and of the *BA*-type slabs (slab no. 2, slab no. 4,…, slab no. 12)

	Slab no. (1), (3), (5), (7), (9), (11) *AB*-type				Slab no. (2), (4), (6), (8), (10), (12) *BA*-type			
	x	y	z	Occ	x	y	z	Occ
M	0.0000	0.0000	0.0000	1.00	0.0000	0.0000	0.0000	1.00
O(1)	2/3	1/3	−0.1100	1.00	2/3	1/3	0.1100	1.00
O(2)	1/3	2/3	0.1100	1.00	1/3	2/3	−0.1100	1.00

The cell parameters used are $a_{hex} = b_{hex} = 2.8035\,\text{Å}$ and $c_{hex} = 9.540\,\text{Å}$.

Table 2
Structural model used for the calculation of the XRD patterns for O2–LiMO_2 with stacking faults, the nucleation centers being only associated to one type of slabs

(i)→(j)	α_{ij}	R_{ij}		
		R_{xij}	R_{yij}	R_{zij}
(1)→(2)	$(1 - P_t)$	1/3	2/3	0.5000
(1)→(4)	P_t	2/3	1/3	0.5000
(2)→(1)	1	2/3	1/3	0.5000
(4)→(1)	1	1/3	2/3	0.5000

The translation probabilities (α_{ij}) and stacking vectors (R_{ij}: R_{xij}, R_{yij}, R_{zij}) are associated to the stacking of the slabs no. *j* above the slabs no. *i*. The probability of defects P_t varies from 0% to 100%, every 2%.

(*BA* for example) could be nucleation center of the P2→O2 transition. An example of P2→O2 transition in this case is given in Fig. 4. Note that for an easier understanding of the slabs gliding, the involved NaO$_6$ trigonal prisms and LiO$_6$ octahedra were drawn with the same size along the c_{hex} direction of the crystal. From these nucleation centers (indicated by the arrows), that are randomly distributed in the crystal, one MO_2 slab over two glides either by (1/3,2/3,0) or by (2/3,1/3,0), leading thus to the formation of blocks of O2-type structure, as shown in the right of Fig. 4b.

In the ideal O2 structure (*AB CB* oxygen packing), the MO_6 octahedra share on one side a face with an LiO$_6$ octahedron and on other side three edges with three LiO$_6$ octahedra. Such environments are highlighted in Fig. 4b by polyhedra drawn with bold lines. But, as also shown in Fig. 4b by hatched polyhedra, two types of defects can be locally observed at the junction between two O2-type blocks that have been obtained through glidings in the opposite ((1/3,2/3,0) or (2/3,1/3,0)) directions. The first type of defects is characterized by an *CB AB AC* oxygen packing: the MO_6 octahedra share faces with the adjacent LiO$_6$ octahedra. The second type of defects is characterized by an *AC AB CB* oxygen packing: the MO_6 octahedra share edges with the adjacent LiO$_6$ octahedra.

The simulation of the corresponding XRD patterns for O2–LiMO_2 with stacking faults was performed using the DIFFaX software. This software has been developed to modelize defects in zeolite structures, but it can be
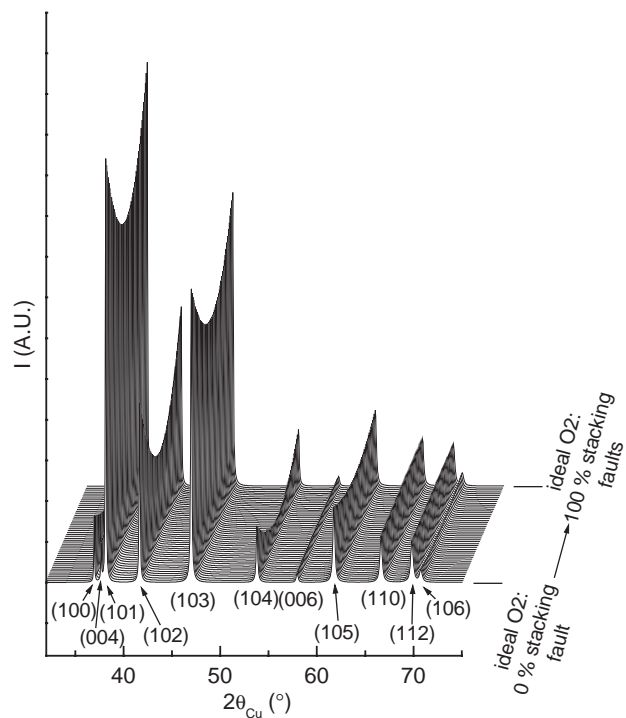

Fig. 6. XRD patterns calculated for O2–LiMO_2 with stacking faults, considering that the nucleation centers are only associated to one type of slabs (*AB* or *BA*). The gliding vectors are (1/3,2/3,0) or (2/3,1/3,0). The (002) line not shown in the figure is not affected by the defects.

used for all structures than can be described as layered structures. In the DIFFaX software, three types of parameters are necessary to describe structures with defects: the slabs, and the stacking vectors and transition probabilities associated. The probability that a specific slab to slab translation occurs in the sequence is weighted by the translation probabilities (α_{ij}), whereas the position of a slab in the sequence is defined by the stacking vector (R_{ij}), always in comparison to the previous slab.

As shown in Fig. 5a, two different slabs are needed to modelize the ideal O2 structure obtained from P2$-$Na$_{0.70}MO_2$ by the gliding of one slab over two by (1/3, 2/3, 0) (an *AB*-type slab (1) and a *BA*-type slab (2)). Furthermore, in order to form the *AB CB* and *CB AB* oxygen packings, it is necessary to associate the (1/3, 2/3, $c_{hex.}$/2) and (2/3, 1/3, $c_{hex.}$/2) stacking vectors
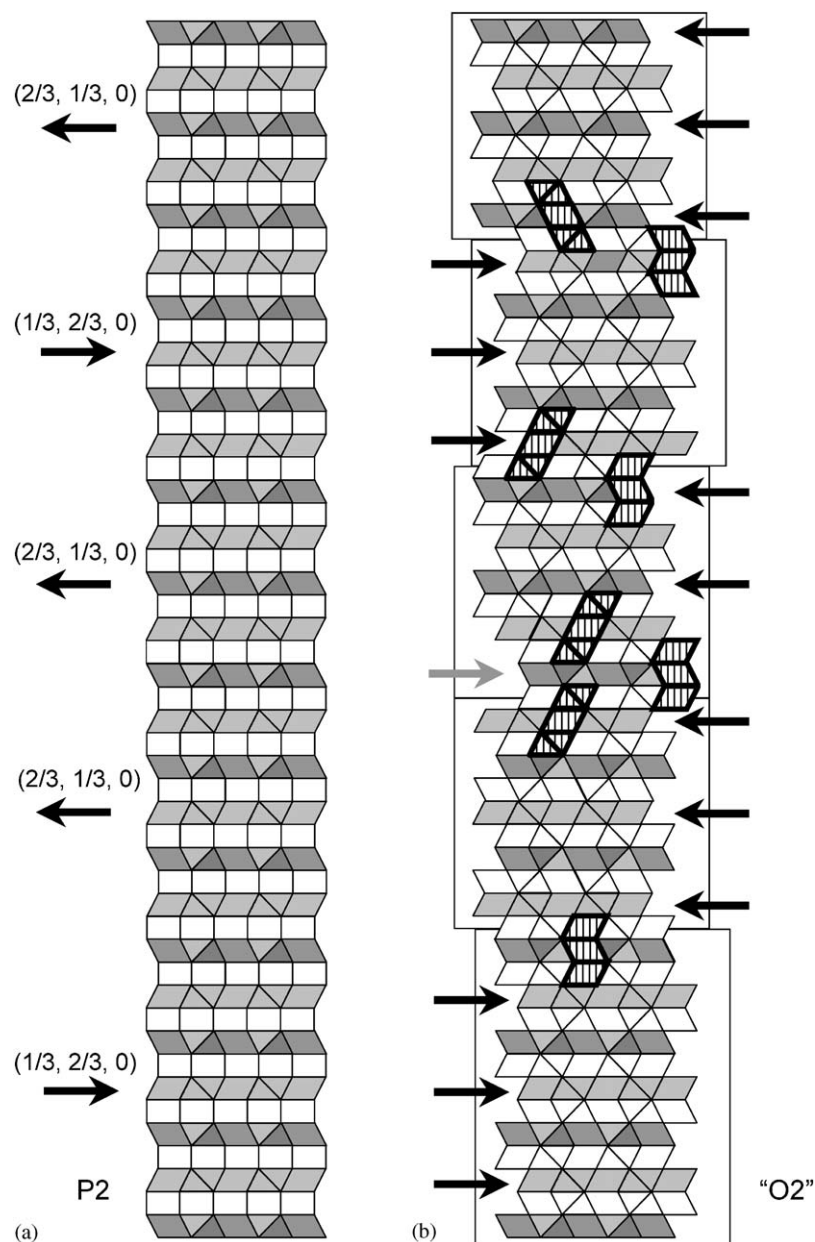
Fig. 7. An example of P2→O2 transition section along the (110) plane. The lighter slabs are *BA*-type slabs whereas the darker slabs are *AB*-type slabs. The nucleation centers are associated to both types of slabs (*AB* or *BA*), the gliding vectors being (1/3,2/3,0) or (2/3,1/3,0). The defects at the junction between two O2 domains are highlighted with hatched polyhedra. Black arrows represent the gliding expected for a given growth domain and the gray ones the gliding necessary to prevent the formation of *AB BA*-type defects. Note that, for convenience, the sodium prisms have been drawn with the same height as the lithium octahedra.

to the **(1)→(2)** and **(2)→(1)** slab stackings, respectively. Because this O2 structure is ideal, the probabilities (α_{ij}) associated to those translations are always equals to 1. In order to avoid any misunderstanding, it is fundamental to specify that the gliding vector corresponds to the slab displacement during the P2→O2 transition, while the stacking vector allows to build a given structure in DIFFaX program: it characterizes the translation of a given slab required to generate the next one.

Now, if we consider the formation of the O2 structure obtained from P2–Na$_{0.7}$MO$_2$ by the gliding of one slab over two by (2/3,1/3,0), the stacking vectors associated to the slab gliding are different: in order to form the *AB AC* and *AC AB* oxygen packings (2/3,1/3,$c_{hex.}$/2) and (1/3,2/3,$c_{hex.}$/2) stacking vectors were associated to the **(1)→(2)** and **(2)→(1)** slab stackings, respectively. In that case, because the O2 structure is also ideal, the probabilities associated to the **(1)→(2)** and **(2)→(1)** are equals to 1.
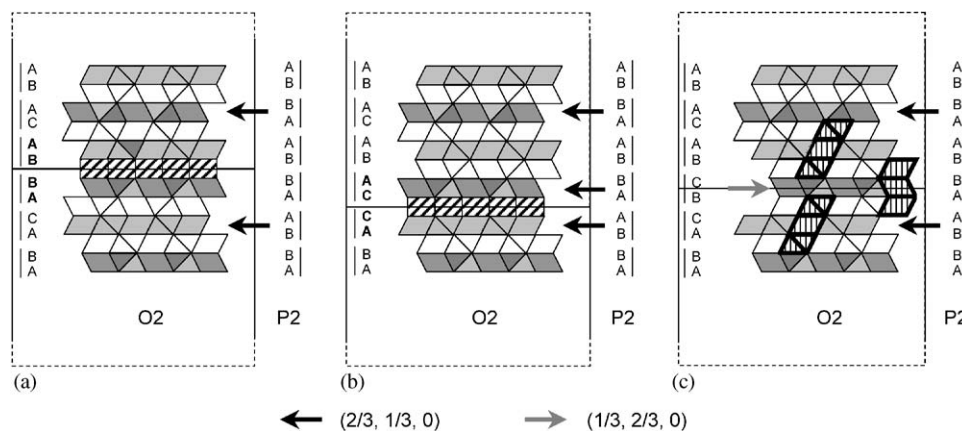
Fig. 8. Projection along the (110) direction of the junction between two O2 blocks obtained by the gliding in the same direction of *AB*-type slabs (for the first) and *BA*-type slabs (for the second). (a) and (b) show stacking with *AB BA*-type defects, whereas in (c) these defects are prevented through a slab gliding in the opposite direction. Black arrows represent the (2/3, 1/3, 0) gliding expected for a given growth domain and the gray ones the (1/3,2/3,0) gliding, necessary to prevent the formation of *AB BA*-type defects.

Table 3
Structural model used for the calculation of the XRD patterns for O2–LiMO_2 with stacking faults, the nucleation centers being associated to both types of slabs

(i)→(j)	α_{ij}	R_{ij}		
		R_{xij}	R_{yij}	R_{zij}
(1)→(2)	$(1 - P_t)$	1/3	2/3	0.5000
(1)→(10)	P_t	2/3	1/3	0.5000
(2)→(1)	$(1 - P_t)$	2/3	1/3	0.5000
(2)→(9)	P_t	1/3	2/3	0.5000
(3)→(6)	$(1 - P_t)$	1/3	2/3	0.5000
(3)→(8)	P_t	2/3	1/3	0.5000
(4)→(5)	$(1 - P_t)$	2/3	1/3	0.5000
(4)→(7)	P_t	1/3	2/3	0.5000
(5)→(4)	$(1 - P_t)$	1/3	2/3	0.5000
(5)→(12)	P_t	2/3	1/3	0.5000
(6)→(3)	$(1 - P_t)$	2/3	1/3	0.5000
(6)→(11)	P_t	1/3	2/3	0.5000
(7)→(2)	$(1 - P_t)$	2/3	1/3	0.5000
(7)→(10)	P_t	1/3	2/3	0.5000
(8)→(1)	P_t	1/3	2/3	0.5000
(8)→(9)	$(1 - P_t)$	2/3	1/3	0.5000
(9)→(6)	P_t	2/3	1/3	0.5000
(9)→(8)	$(1 - P_t)$	1/3	2/3	0.5000
(10)→(5)	P_t	1/3	2/3	0.5000
(10)→(7)	$(1 - P_t)$	2/3	1/3	0.5000
(11)→(4)	P_t	2/3	1/3	0.5000
(11)→(12)	$(1 - P_t)$	1/3	2/3	0.5000
(12)→(3)	P_t	1/3	2/3	0.5000
(12)→(11)	$(1 - P_t)$	2/3	1/3	0.5000

The translation probabilities (α_{ij}) and stacking vectors (R_{ij}: R_{xij}, R_{yij}, R_{zij}) are associated to the stacking of the slabs no. *j* above the slabs no. *i*. The probability of defects P_t varies from 0% to 100%, every 2%.

To simulate the XRD patterns when defects are present in the structure, we have to consider the structural description in a more general point of view to use the DIFFaX software. Depending on the stacking

vector, an *BC* or *CA* slab. These slabs are named using an odd number **(1)**, **(3)**, **(5)**, **(7)**, **(9)** and **(11)**. *BA*-type slab can also lead to a *CB* or *AC* slab. These slabs are named using an even number **(2)**, **(4)**, **(6)**, **(8)**, **(10)** and **(12)**. In this structure, 12 slabs are required to describe the packing in the most general case. As previously mentioned in the peculiar case of the ideal structure only slab **(1)** and **(2)** were required.

As shown in Fig. 5b, if we want to take into account the formation of possible defects on a specific type of slabs (here *AB*), we need then one *AB*-type slab **(1)** and two *BA*-type slabs **(2)** and **(4)** (remember that we have considered in this simplified model that only the *BA*-type slab can move). The O2 domains is thus defined by the **(1)→(2)→(1)→(2)→(1)→(2)**... or **(1)→(4)→(1)→(4)→(1)→(4)**... slab series and the defects will be induced by the **(2)→(1)→(4)** and **(4)→(1)→(2)** series. If P_t is the ratio of defects in the structure, it corresponds to the probability to have **(1)→(4)** transition (Fig. 5b) and, therefore, the probability for the **(1)→(2)** transition to occur is $1 - P_t$. Because no defects can appear on *AB*-type slabs the probabilities associated to the **(4)→(1)** and **(2)→(1)** transitions are equal to 1.

The crystals were considered to be characterized by an infinite size and the probability (P_t) of defects to vary between 0% and 100% every 2%. In the program, to describe the shape of the diffraction lines we used a pseudo-voigt function. The u, v, w parameters were those of the experimental P2–$Na_{0.70}CoO_2$ XRD pattern; therefore even if an infinite crystal is assumed from the DiFFaX point of view, the coherence length corresponds to that of the material before exchange reaction. Three slabs were used to describe the structural model, one of the *AB*-type and two of the *BA*-type: the corresponding atomic positions are given in Table 1. Table 2 gives the probability (α_{ij}) for finding slab **(j)**
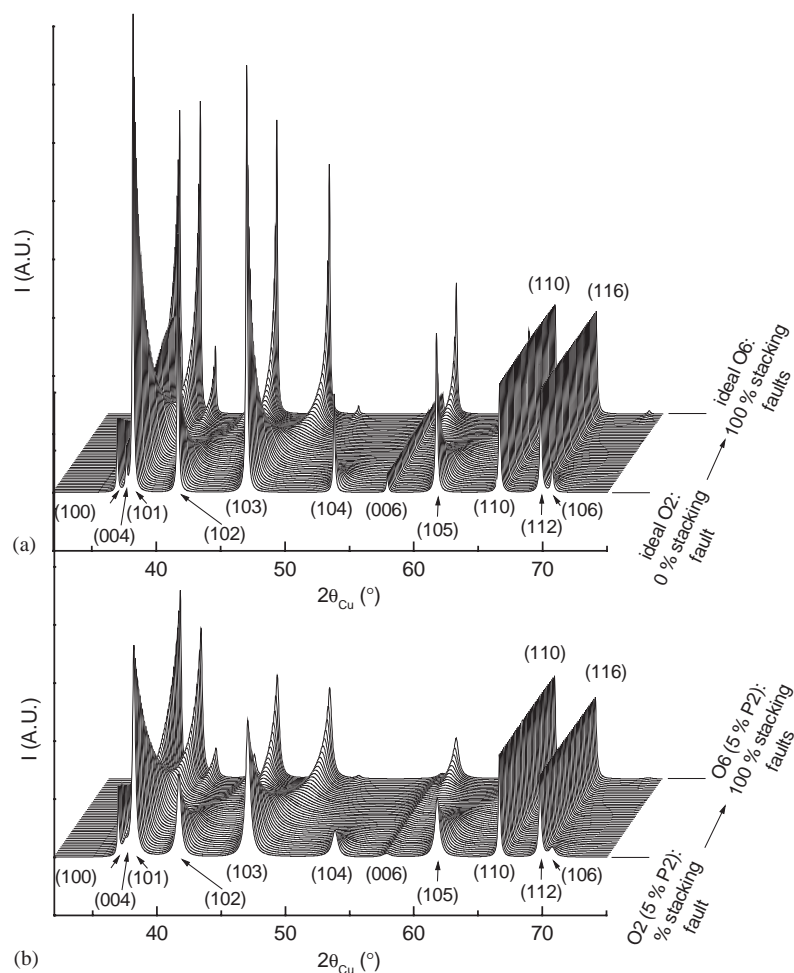
Fig. 9. XRD patterns calculated for O2–LiMO_2 with stacking faults (a) and with stacking faults and 5% trigonal prismatic defects (*AB BA*) (b), considering that the nucleation centers are associated to both types of slabs (*AB* or *BA*). Gliding vectors are (1/3,2/3,0) or (2/3,1/3,0), but without possible formation of prismatic defects (*AB BA*). The (002) line not shown in the figure is not affected by the defects.

located above slab **(i)**, as well as the stacking vector (R_{ij}) that characterizes the position of slab **(j)** versus slab **(i)**. The probabilities that are not given are equal to zero. The simulated XRD patterns are given in Fig. 6. Note that the more disordered structure is obtained for $P_t = 50\%$. Indeed, the structure obtained for $P_t = 100\%$ is also a perfectly ordered structure with an *AB AC* oxygen packing; this structure is identical to the initial O2 structure ($P_t = 0\%$) that is characterized by an *AB CB* oxygen packing. The (00*l*) and (11*l*) diffraction lines are not modified by the presence of defects, whereas the full-width at half-maximum (FWHM) of the (10*l*) peaks increases up to 50% of defects and decreases after.

3.2.2. General case: the two types of slabs are nucleation centers

As the previous model is only a special case (only *BA* slabs were considered to glide) of a more general one, we have then considered that the two different types of slabs (*AB* and *BA*) could be nucleation centers.

Fig. 7 presents one possible scheme for the P2→O2 transition, with the hypothesis that both types of slabs could be nucleation centers. The arrows indicate the gliding of the first slab in the considered domain. The defects at the boundary between two domains are locally the same as those observed for the previous hypothesis, i.e., *CB AB AC* or *AC AB CB*. Nevertheless, an other type of defects (*AB BA*), can theoretically be observed. Indeed, as shown in Fig. 8a, at the junction between two O2 blocks formed through the gliding in the same direction of *BA*-type slabs (for the first) and *AB*-type slabs (for the second), an *AB BA* oxygen packing is locally observed, with trigonal prismatic sites in the interslab space. Note that to our knowledge, the lithium ions due to their small size are not stable in trigonal prismatic sites in such layered oxides. The *AB BA*-type stacking faults would be only due to the presence of residual sodium ions trapped in the structure and they are not expected in the final material. To prevent such defects, a gliding visualized by the gray arrow has to occur locally in opposite direction (Fig. 8c), because

gliding in the same direction would also lead to a trigonal prismatic surrounding *AC CA*-type defect (Fig. 8b).

The principle of the simulation was described previously, but more stacking vectors are needed as the nucleation can appears on each *AB* or *BA*-type slab. The simulation of the corresponding XRD patterns for O2–LiMO_2 with stacking faults has been achieved considering an infinite size for crystals and a probability of defects (P_t) varying between 0% and 100%, every 2%. As *AB* and *BA* slabs play a similar role in the structure, from an energy point of view the probabilities of gliding in the different directions are the same for both types of slab. Therefore, there is a single value for P_t whatever the considered slab related to a defect. The formation of *AB BA*-type defects has been forbidden in a first step. Twelve slabs were used to describe the structural model, six of the *AB*-type **(1)**, **(3)**, **(5)**, **(7)**, **(9)**, **(11)** and six of the *BA*-type **(2)**, **(4)**, **(6)**, **(8)**, **(10)**, **(12)**: the corresponding atomic positions are given in Table 1, whereas the probability (α_{ij}) and the stacking vectors (R_{ij}) are given in Table 3. The probabilities that are not given are zero.

The XRD patterns obtained are given in Fig. 9a. For small amounts of stacking faults, the evolution of the XRD patterns is similar to the one observed in Fig. 6 for

the previous hypothesis, but stronger. The (00*l*) and (11*l*) peaks are not affected by the presence of stacking faults, whereas the FWHM of the (10*l*) diffraction lines increases rapidly up to 50% stacking faults. In that case, the structure obtained for $P_t = 1$, is an O6 structure, with the *AB AC BC BA CA CB AB* oxygen packing. Fig. 10 shows the comparison of the section of the P2 and O6 structures and the involved glidings which occur in the case of a P2→O6 transition. The MO_6 octahedra of one slab over two share edges with adjacent LiO_6 octahedra, whereas the MO_6 octahedra of the other slabs share faces with adjacent LiO_6 octahedra. It is interesting to point out that this unusual O6 stacking was obtained for the first time upon lithium deintercalation from the O2–Li$_x$CoO$_2$ system, in the $0.33 \leqslant x \leqslant 0.42$ composition range [2,5]. More recently, Dahn et al. have obtained this O6-type structure for the Li$_{0.70}$[Mg$_{0.30}$Mn$_{0.70}$]O$_2$ starting material, directly obtained by ion exchange of sodium by lithium from P2–Na$_{0.70}$[Mg$_{0.30}$Mn$_{0.70}$]O$_2$ [11].

In the previous part, the existence of *AB BA* domains was excluded because Li$^+$ are too small to occupy trigonal prismatic sites. Nevertheless, their existence could result from the presence of remaining Na$^+$ ions in the structure. In order to check this hypothesis, a simulation was made with 5% of *AB BA*-type defects.
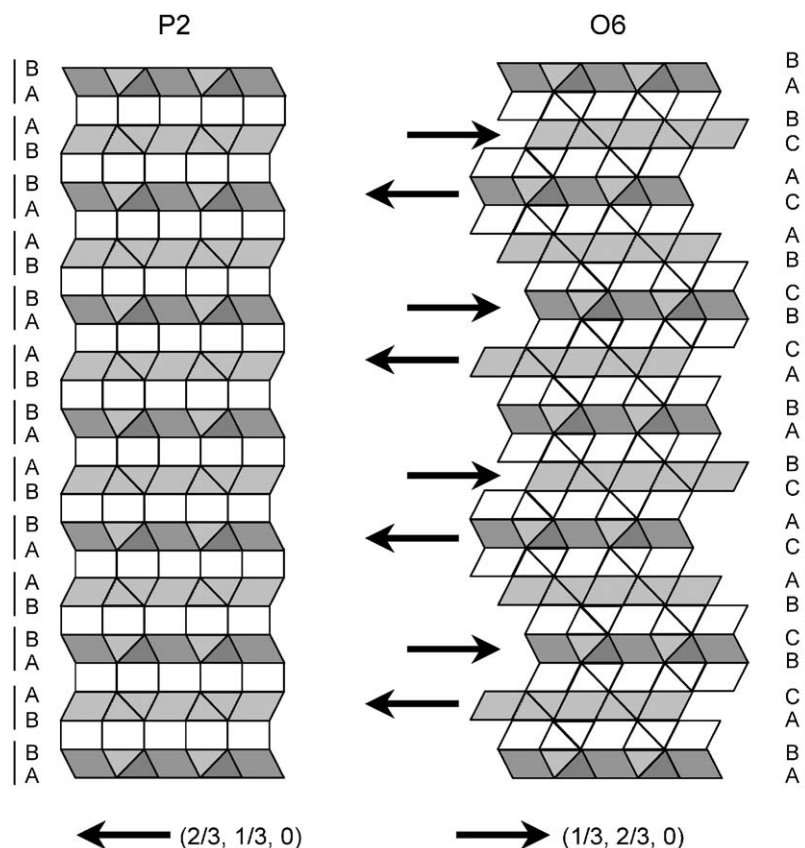

Fig. 10. P2→O6 transition section along (110) plane. The lighter slabs are *BA*-type slabs, whereas the darker slabs are *AB*-type slabs, the gliding vectors (black arrows) being (1/3,2/3,0) or (2/3,1/3,0).

This value of 5% was chosen in reference to the experimental results. Indeed, chemical analyses have shown less than 3.6% of sodium ions remaining in O2–LiCoO$_2$: assuming that trigonal prismatic interslab spaces were occupied like in P2–Na$_{0.7}$CoO$_2$, this leads to 5% of AB BA-type domains in the structure. Note that this value is overestimated because the majority of the sodium ions belongs to residual Na$_x$CoO$_2$. Twelve slabs were used to describe the structural model, six of the AB-type and six of the BA-type: their corresponding atomic positions are given in Table 1, whereas the probability (α_{ij}) and the stacking vectors (R_{ij}) are given in Table 4. The probabilities that are not given are zero. The comparison of Figs. 9a and b shows that the

introduction of a small amount of AB BA-type stacking faults (5%) leads only to a larger broadening of the diffraction lines sensitive to the stacking faults.

3.3. Comparison with the experimental results obtained for the Na$^+$ by Li$^+$ exchange in P2–Na$_{0.7}$CoO$_2$

The experimental XRD pattern of LiCoO$_2$ has been compared with those simulated for 0%, 1%, 2%, 4% and 6% of stacking faults (in the general case AB and BA gliding and no AB BA-type defects). The best fit is obtained for 1% of stacking faults. Fig. 11 shows the comparison of the O2–LiCoO$_2$ experimental pattern and the "1% defects" one. On insert on this figure, the (102) and (103) diffraction lines which are very sensitive to the presence of defects are represented. The comparison of the FWHM values for all diffraction lines shows clearly that the amount of defects in the material is close to 1%. These simulations have shown that the amount of stacking faults is very small in O2–LiCoO$_2$ and, therefore, that the growth from a nucleation center during the ion exchange of sodium by lithium in P2–Na$_{0.70}$CoO$_2$ is faster than the multiplication of the nucleation centers.

4. Discussion and conclusion

In order to explain why the growing of an homogenous O2 domain in P2–Na$_{0.7}$CoO$_2$ crystals, when one first CoO$_2$ slab has glided, is faster than the nucleation, we have to consider the stresses induced within the structure by the gliding. During the Li$^+$/Na$^+$ exchange reaction, there is a decrease of the in-slab Co–Co distance which is equal to the a_{hex} parameter ($a_{hex} = 2.833$ Å for P2–Na$_{0.70}$CoO$_2$ and $a_{hex} = 2.804$ Å for O2–LiCoO$_2$). When the first CoO$_2$ slab has glided, it is surrounded by two Li$^+$ ion layers like in O2–LiCoO$_2$ (Fig. 2c). Therefore, we can assume that the contraction of this CoO$_2$ slab occurs, leading to a decrease of the Co–Co distances. The two next CoO$_2$ slabs, which are surrounded by a Li$^+$ ion layer on one side and by a Na$^+$ ion layer on the other side, are destabilized. In order to stabilize locally the structure, the next CoO$_2$ slabs on each side glide in the same direction (to avoid only face sharing between CoO$_6$ and its neighboring LiO$_6$ octahedra), resulting in an increase of the O2 domain thickness.

We have proposed a model for the P2→O2 transition based on a nucleation-growing process. Interestingly, it has shown that depending on the ratio between the growing and nucleation speeds, O2, O6 or faulted structures are obtained after sodium by lithium ion exchange in P2 crystals. These results allow to analyze the formation of the metastable lamellar phases obtained from P2 phases by ionic exchange. XRD
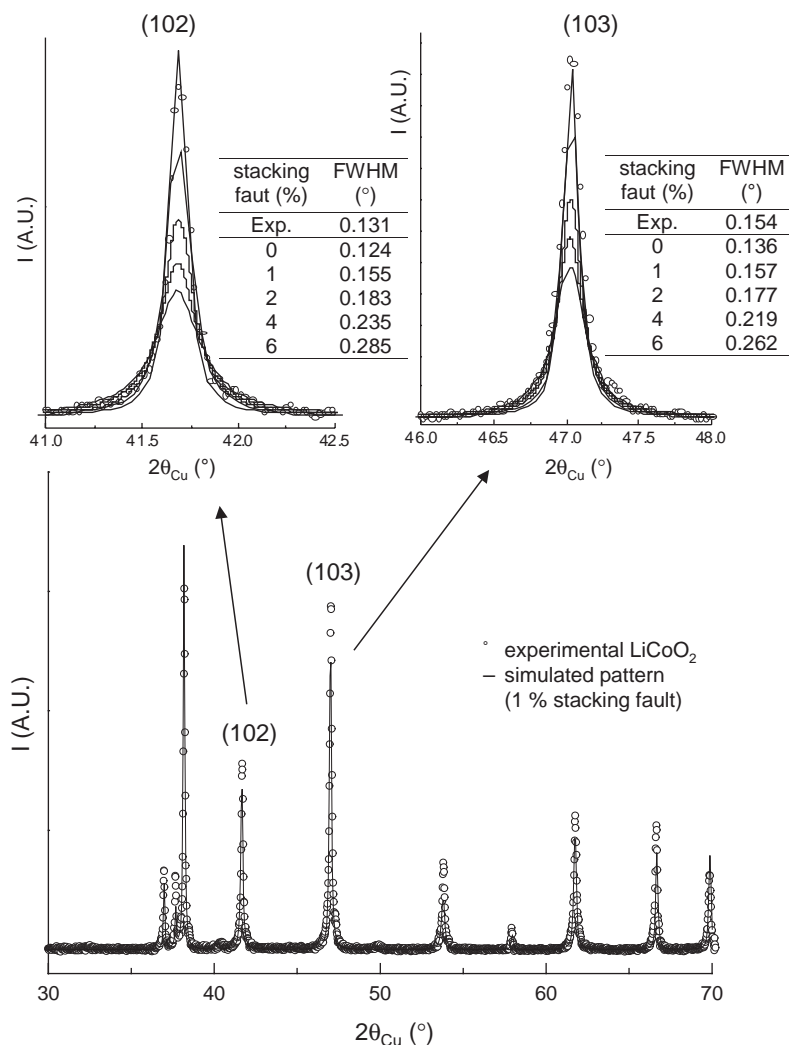
Table 4
Structural model used for the calculation of the XRD patterns for O2–LiMO_2 with stacking faults, the nucleation centers being associated to both types of slabs

(i)→(j)	α_{ij}	R_{ij}		
		R_{xij}	R_{yij}	R_{zij}
(1)→(2)	$(0.95 - P_t)$	1/3	2/3	0.5000
(1)→(6)	0.05	0.0000	0.0000	0.5719
(1)→(10)	P_t	2/3	1/3	0.5000
(2)→(1)	$(0.95 - P_t)$	2/3	1/3	0.5000
(2)→(5)	0.05	0.0000	0.0000	0.5719
(2)→(9)	P_t	1/3	2/3	0.5000
(3)→(4)	0.05	0.0000	0.0000	0.5719
(3)→(6)	$(0.095 - P_t)$	1/3	2/3	0.5000
(3)→(8)	P_t	2/3	1/3	0.5000
(4)→(3)	0.05	0.0000	0.0000	0.5719
(4)→(5)	$(0.095 - P_t)$	2/3	1/3	0.5000
(4)→(7)	P_t	1/3	2/3	0.5000
(5)→(2)	0.05	0.0000	0.0000	0.5719
(5)→(4)	$(0.095 - P_t)$	1/3	2/3	0.5000
(5)→(12)	P_t	2/3	1/3	0.5000
(6)→(1)	0.05	0.0000	0.0000	0.5719
(6)→(3)	$(0.095 - P_t)$	2/3	1/3	0.5000
(6)→(11)	P_t	1/3	2/3	0.5000
(7)→(2)	P_t	2/3	1/3	0.5000
(7)→(10)	$(0.95 - P_t)$	1/3	2/3	0.5000
(7)→(12)	0.05	0.0000	0.0000	0.5719
(8)→(1)	P_t	1/3	2/3	0.5000
(8)→(9)	$(0.95 - P_t)$	2/3	1/3	0.5000
(8)→(11)	0.05	0.0000	0.0000	0.5719
(9)→(6)	P_t	2/3	1/3	0.5000
(9)→(8)	$(0.95 - P_t)$	1/3	2/3	0.5000
(9)→(10)	0.05	0.0000	0.0000	0.5719
(10)→(5)	P_t	1/3	2/3	0.5000
(10)→(7)	$(0.95 - P_t)$	2/3	1/3	0.5000
(10)→(9)	0.05	0.0000	0.0000	0.5719
(11)→(4)	P_t	2/3	1/3	0.5000
(11)→(8)	0.05	0.0000	0.0000	0.5719
(11)→(12)	$(0.95 - P_t)$	1/3	2/3	0.5000
(12)→(3)	P_t	1/3	2/3	0.5000
(12)→(7)	0.05	0.0000	0.0000	0.5719
(12)→(11)	$(0.95 - P_t)$	2/3	1/3	0.5000

The translation probabilities (α_{ij}) and stacking vectors (R_{ij}: R_{xij}, R_{yij}, R_{zij}) are associated to the stacking of the slabs no. j above the slabs no. i. The probability of defects P_t varies from 0% to 100%, every 2%. The probability of AB BA defects is maintained to 5%.

stacking faut (%)	FWHM (°)
Exp.	0.131
0	0.124
1	0.155
2	0.183
4	0.235
6	0.285

stacking faut (%)	FWHM (°)
Exp.	0.154
0	0.136
1	0.157
2	0.177
4	0.219
6	0.262

Fig. 11. Comparison between the experimental XRD pattern of O2–LiCoO$_2$ and the patterns calculated for O2–LiCoO$_2$ in the hypothesis of 1% stacking faults. The nucleation centers are associated to both types of slabs (*AB* or *BA*). No trigonal prismatic defects (*AB BA*) were considered. Enlargement of the (102) and (103) diffraction lines with the patterns calculated for O2–LiCoO$_2$ in the hypothesis of 0%, 1%, 2%, 4% and 6% stacking faults and the corresponding FWHMs is also reported.

patterns simulation and their comparison with the experimental O2–LiCoO$_2$ one have shown that there was almost no defects in the O2–LiCoO$_2$ structure obtained by ion exchange in water. Therefore, this study has shown that the growth of the O2 domains in the P2–Na$_{0.7}$CoO$_2$ crystals is faster than the formation of nucleation centers.

In the next companion paper, we will follow the P2–Na$_{0.7}$CoO$_2$→O2–LiCoO$_2$ exchange reaction in situ by X-ray diffraction to check the previous conclusions and to determine the mechanism of the reaction.

Acknowledgments

References

[1] C. Delmas, J.J. Braconnier, P. Hagenmuller, Mater. Res. Bull. 17 (1982) 117.

[2] A. Mendiboure, C. Delmas, P. Hagenmuller, Mater. Res. Bull. 19 (1984) 1383.

[3] C. Delmas, C. Fouassier, P. Hagenmuller, Physica 99B (1980) 81.

[4] J.M. Paulsen, C.L. Thomas, J.R. Dahn, J. Electrochem. Soc. 146 (1999) 3560.

[5] J.M. Paulsen, J.R. Mueller-Neuhaus, J.R. Dahn, J. Electrochem. Soc. 147 (2000) 508–516.

[6] J.M. Paulsen, C.L. Thomas, J.R. Dahn, J. Electrochem. Soc. 147 (2000) 2862–2867.

[7] J.M. Paulsen, J.R. Dahn, J. Electrochem. Soc. 147 (2000) 2478–2485.

[8] Z.H. Lu, J.R. Dahn, J. Electrochem. Soc. 148 (2001) A237.

[9] Z.H. Lu, R.A. Donaberger, C.L. Thomas, J.R. Dahn, J. Electrochem. Soc. 149 (2002) A1083–A1091.

[10] Z.H. Lu, J.R. Dahn, Chem. Mater. 13 (2001) 2078.

[11] J.M. Paulsen, R.A. Donaberger, J.R. Dahn, Chem. Mater. 12 (2000) 2257–2267.

[12] D. Carlier, I. Saadoune, E. Suard, L. Croguennec, M. Ménétrier, C. Delmas, Solid State Ionics 144 (2001) 263–276.

[13] C. Fouassier, G. Matejka, J.M. Reau, P. Hagenmuller, J. Solid State Chem. 6 (1973) 532.

[14] R.D. Shannon, C.T. Prewitt, Acta Crystallogr. B 25 (1969) 925.